Journal of Physics:
Condensed Matter

PAPER • **OPEN ACCESS**

From weak- to strong-coupling superconductivity in the AlB_2-type solid solution $SrGa_{1-x}Al_xGe$ with honeycomb layers

To cite this article: Dorota I Walicka *et al* 2025 *J. Phys.: Condens. Matter* **37** 045704

OPEN ACCESS
IOP Publishing
Journal of Physics: Condensed Matter
J. Phys.: Condens. Matter **37** (2025) 045704 (10pp)
https://doi.org/10.1088/1361-648X/ad8c0b

From weak- to strong-coupling superconductivity in the AlB_2-type solid solution $SrGa_{1-x}Al_xGe$ with honeycomb layers

Dorota I Walicka[1,2,3,*], Olivier Blacque[2], Tomasz Klimczuk[4,5] and Fabian O von Rohr[1,*]

[1] Department of Quantum Matter Physics, University of Geneva, CH-1211 Geneva, Switzerland
[2] Department of Chemistry, University of Zurich, CH-8057 Zurich, Switzerland
[3] Laboratory for Neutron Scattering and Imaging, PSI Center for Neutron and Muon Sciences, CH-5232 Villigen PSI, Switzerland
[4] Faculty of Applied Physics and Mathematics, Gdansk University of Technology, 80-233 Gdansk, Poland
[5] Advanced Materials Center, Gdansk University of Technology, 80-233 Gdansk, Poland

E-mail: dorota.walicka@psi.ch and fabian.vonrohr@unige.ch

Received 30 August 2024, revised 14 October 2024
Accepted for publication 28 October 2024
Published 12 November 2024

Abstract

We report on the structure and the superconducting properties of 9-electron 111 compounds with honeycomb layers, namely SrGaGe, SrAlGe, and the $SrGa_{1-x}Al_xGe$ solid solution. By means of single-crystal x-ray diffraction we show that, on one hand, SrGaGe crystallizes into the centrosymmetric *P6/mmm* space group ($a = 4.2555(2)$ Å, $c = 4.7288(2)$ Å) with statistical disorder in the $[GaGe]_6^{2-}$ honeycomb layers. On the other hand, we confirm that SrAlGe crystallizes in a non-centrosymmetric space group, namely $P\bar{6}m2$ ($a = 4.2942(1)$ Å, $c = 4.7200(2)$ Å) with fully ordered $[AlGe]_6^{2-}$ honeycomb layers. By using magnetization and specific heat measurements, we show that the superconducting properties of SrGaGe and SrAlGe differ significantly from each other. SrGaGe is a superconductor with a critical temperature of $T_c = 2.6$ K falling into the weak coupling limit, while SrAlGe has a $T_c = 6.7$ K and can be classified in the strong coupling limit. By realizing the $SrGa_{1-x}Al_xGe$ solid solution, we were able to investigate the transition between the different crystal structures as well as the evolution of the electronic properties. We show that the transition from the weak-to strong-coupling superconductivity in this system is likely associated with the disorder-to-order transition of the honeycomb layer, along with the loss of the inversion center in the crystal structure.

* Authors to whom any correspondence should be addressed.

Supplementary material for this article is available online

Keywords: superconductivity, honeycomb layers, non-centrosymmetric superconductors, disorder

1. Introduction

Superconductivity in materials with honeycomb layers has attracted significant interest, particularly following the discovery of unconventional superconductivity in magic-angle bilayer graphene [1], or also in the context of superconductivity in AlB_2 materials, such as MgB_2 [2]. One particular opportunity in AlB_2-type superconductors is the possible loss of centrosymmetry in the structure, by ordering the atoms on the honeycomb layers. Superconductors with non-centrosymmetric structures are of interest as they can host antisymmetric spin–orbit coupling, which can lead to the mixing of the spin-singlet and spin-triplet components [3, 4]. Non-centrosymmetric superconductors have been extensively studied, most prominently the heavy fermion superconductor $CePt_3Si$ [5]. Several non-centrosymmetric superconductors have been considered as candidates for topological superconductivity [6].

Among ternary AlB_2-type superconductors with honeycomb layers, SrPtAs has been most prominently discussed. This compound crystallizes in the centrosymmetric space group $P6_3/mmc$. Interestingly, SrPtAs is locally non-centrosymmetric, and based on this, it has been proposed to host intrinsic topological superconductivity with a chiral $d+id$ gap and a critical temperature of $T_c = 2.4$ K [7–9].

The highest critical temperatures in ternary AlB_2-type superconductors are found in 9-electron 111 compounds [10]. Within this group of compounds CaAlSi has been reported to have a critical temperature of $T_c = 7.8$ K. The crystal structure of CaAlSi is related to the AlB_2 structure, but it is more complex, with buckling of the honeycomb layers, indicating a versatile interplay between structure and superconductivity in these materials [11–17].

The here investigated SrGaGe and SrAlGe are both 9-electron 111 superconductors, related to the AlB_2 structure with honeycomb layers. For SrGaGe, two crystal structures have previously been reported. It was reported to crystallize into the $P6_3/mmc$ space group with a buckled 4 H structure consisting of 4 alternating layers [18] and the $P6/mmm$ space group [10], where a fivefold modulation of the stacking sequence has been proposed. SrAlGe has been reported to crystallize in the $P\bar{6}m2$ space group with planar and ordered honeycomb layers [10]. Preliminary data for both compounds show superconductivity with $T_c = 2.6$ K and $T_c = 6.7$ K for SrGaGe and SrAlGe [10], respectively. The relatively high transition temperature of SrAlGe was attributed by first principle calculations to the enhanced electron–phonon coupling along the c direction [19]. It is worth noting that the $P\bar{6}m2$ space group does not have an inversion center, which makes SrAlGe a non-centrosymmetric superconductor with honeycomb layers.

In this work, we investigate the structural and superconducting properties of these 9-electron 111 compounds, namely SrGaGe and SrAlGe and the $SrGa_{1-x}Al_xGe$ solid solution. Specifically, we show a different structural model for SrGaGe and unambiguously describe this compound as a bulk superconductor in the weak coupling limit. Moreover, we confirm that SrAlGe crystallizes in the fully ordered $P\bar{6}m2$ space group, and we show that this compound is a strong coupling superconductor. We also synthesized the continuous $SrGa_{1-x}Al_xGe$ solid solution, for which we observe a structural transition from disordered to ordered honeycomb layers upon substitution of Ga for Al. The continuous transition from weak to strong electron–phonon coupling within this solid solution appears to be connected to a disorder-to-order transition and the loss of the inversion center on the honeycomb layer.

2. Methods

Synthesis: All samples were prepared by arc melting stoichiometric amounts of Sr (99.99% Aldrich), Al (99.9995% Acros Organic), Ga (Roth, 99.999%) and Ge (Alfa Aesar, 99.999%) under purified argon atmosphere, on a water-cooled copper plate using a tungsten tip. The samples were melted shortly, in order to avoid the evaporation of Sr but multiple times with flipping the sample over, after every firing. This was performed to ensure the maximum homogeneity of the products. The melted ingot was sealed in a quartz tube, annealed for 24 h at 830 °C, and eventually cooled down to room temperature with a rate of 30 °C/h. The samples were handled inside an argon filled glovebox, as they were found to be air and moisture sensitive.

Diffraction: Powder x-ray Diffraction (PXRD) data were collected on a STOE STADIP diffractometer equipped with a Ge-monochromator using Cu–$K_{\alpha 1}$ radiation ($\lambda = 1.540\,51$ Å) in the 2θ range 5°–90°. The data were analyzed using the FULLPROF program package [20] employing LeBail fits.

Single-crystal x-ray diffraction (SXRD) data were collected at 160(1) K on a Rigaku OD SuperNova/Atlas area-detector diffractometer and a Rigaku OD Synergy/Hypix diffractometer using Cu $K_{\alpha 1}$ radiation ($\lambda = 1.54184$ Å) from a micro-focus x-ray source and an Oxford Instruments Cryojet XL cooler. The selected suitable single crystal was mounted using polybutene oil on a flexible loop fixed on a goniometer head and immediately transferred to the diffractometer. Pre-experiment, data collection, data reduction and analytical absorption correction [21] were performed with the program suite CrysAlisPro. Using Olex2 [22], the structure was solved with the SHELXT [23] small molecule structure solution program and refined with the SHELXL2018/3 program

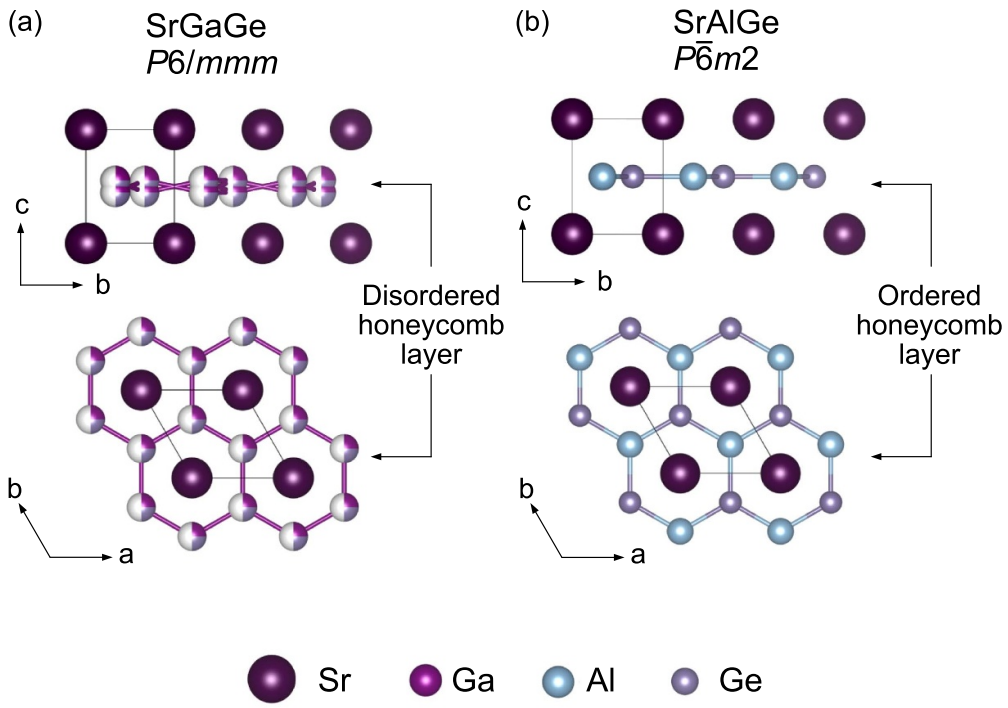

Figure 1. Obtained structural model from SXRD for (a) SrGaGe and (b) SrAlGe. SrGaGe crystallizes into the *P*6/*mmm* space group with disordered honeycomb layers, while SrAlGe crystallizes into *P*$\bar{6}$*m2* space group with planar honeycomb layers. Both compounds are shown along the *a* and *c* directions.

package [24] by full-matrix least-squares minimization of F^2. PLATON [25] was used to check the result of the x-ray analysis.

Elemental characterization: Elemental analysis was performed by energy dispersive x-ray spectroscopy (EDS) using a Jeol JSM-7600 *F* field emission scanning electron microscope equipped with an x-ray detector X-MAX80, AZTec Advanced, Oxford. Multiple spectra for each sample were collected at a working distance of 15 mm and an applied voltage of 10 kV.

Physical properties: Magnetic measurements were performed on a quantum design magnetic properties measurement system (MPMS3) equipped with a vibrating sample magnetometer (VSM) option and a 7 T magnet, as well as on a quantum design physical property measuring system (PPMS) Evercool II equipped with a VSM option and a 9 T magnet. Samples were of an arbitrary shape and in a mass range between 8–25 mg. Heat capacity measurements were performed using a PPMS Evercool II in a magnetic field ranging from 0 T to 2.5 T using the two-τ time-relaxation method. The sample was mounted on the measurement platform using Apiezon N grease.

3. Results

3.1. Structure and composition

Samples of SrGaGe, SrAlGe, and the whole $SrGa_{1-x}Al_xGe$ solid solution were obtained as silvery shinny ingots with metallic luster. Composition and stoichiometry of the samples were confirmed by EDS, as shown in figure S1 and table S1 in supplemental material (SM). The determined experimental composition was found to be very close to the targeted one, hence a nominal value of *x* will be used throughout the text. All members of the solid solution were found to be highly air-sensitive. Their stability varies from SrGaGe, which is stable up to few hours, to SrAlGe which decomposes immediately after exposure to air.

We have performed SXRD measurements for the end members of the solid solution, SrGaGe and SrAlGe, respectively. For the other compounds of the solid solution refining three atoms with similar electron density, i.e. Ga, Al, and Ge, at one crystallographic position would be unreliable by x-ray diffraction. We find that SrGaGe crystallizes in the *P*6/*mmm* space group, with unit cell parameters: $a = 4.2555(2)$ Å and $c = 4.7288(2)$ Å, where the positions in the honeycomb layer are stochastically occupied by Ga and Ge atoms, with a Ga-Ge distance of 2.5079(4) Å. An additional positional disorder was observed within the honeycomb layer along the *c*-axis, which can be interpreted as a slight buckling of the honeycomb layers. Our solution of the SrGaGe structure differs from earlier reports. Czybulka *et al* [18] described powder data obtained from Guinier and Straumanis images. They report that SrGaGe crystallizes into the $P6_3/mmc$ space group with unit cell parameters $a = 4.250(1)$ Å and $c = 18.630(3)$ Å (4 H structure). However, no further structural details are provided. This structure type is four-fold enlarged along *c* direction in comparison to the AlB_2-type structure, with buckled Ga/Ge layers, alternately stacked on top of each other, where Ga and Ge atoms occupy the distinct crystallographic positions. One unit of the

Table 1. Details of the SXRD measurements and of the structural refinement for SrGaGe and SrAlGe.

Single-crystal data for SrGaGe and SrAlGe		
Composition	SrGaGe	SrAlGe
CCDC/FIZ	2368 347	2368 346
Formula weight (g mol^{-1})	229.93	187.19
Temperature [K]	160(1)	160(1)
Crystal system	hexagonal	hexagonal
Space group	*P6/mmm*	$P\bar{6}m2$
a [Å]	4.2555(2)	4.2942(1)
b [Å]	4.2555(2)	4.2942(1)
c [Å]	4.7288(2)	4.7200(2)
α [°]	90	90
β [°]	90	90
γ [°]	120	120
Volume [Å^3]	74.162(8)	75.377(5)
Z	1	1
ρ_{calc} (g cm^{-3})	5.143	4.124
μ (mm^{-1})	42.987	35.701
$F(000)$	101.0	83.0
Crystal size (mm^{-3})	0.01 × 0.01 × 0.01	0.08 × 0.07 × 0.02
Radiation	Cu–Kα (λ = 1.54 184 Å)	Cu–Kα (λ = 1.541 84)
2θ range for data collection [°]	9.383 to 73.456	18.800 to 152.252
Index ranges	$-4 \leqslant h \leqslant 4$	$-5 \leqslant h \leqslant 4$
	$-5 \leqslant k \leqslant 5$	$-5 \leqslant k \leqslant 5$
	$-5 \leqslant l \leqslant 5$	$-3 \leqslant l \leqslant 5$
Reflections collected	829	600
Independent reflections	47 [R_{int} = 0.0366	85 [R_{int} = 0.0199
	R_{sigma} = 0.0112]	R_{sigma} = 0.0088]
Data/restraints/parameters	47/0/7	85/0/9
Goodness-of-fit on F^2	1.244	1.276
Final R indexes [I $\geqslant 2\,\sigma$ (I)]	R_1 = 0.0085	R_1 = 0.0135
	wR_2 = 0.0205	wR_2 = 0.0392
Final R indexes [all data]	R_1 = 0.0085	R_1 = 0.0143
	wR_2 = 0.0205	wR_2 = 0.0394
Largest diff. peak/hole (eÅ^{-3})	0.26/−0.20	0.28/−0.42

Table 2. Wyckoff positions, atomic coordinates, equivalent isotropic displacement parameters, and occupancies of the atoms in SrGaGe and SrAlGe as obtained by SXRD.

SrGaGe						
Atom	Symbol	x	y	z	U_{ISO}	Occ.
Sr1	1*b*	0	0	0	0.0089(2)	1
Ga1	4*h*	1/3	2/3	0.5532	0.0147(4)	0.25
Ge1	4*h*	1/3	2/3	0.5532	0.0147(4)	0.25
SrAlGe						
Sr1	1*a*	0	0	0	0.0108(4)	1
Al1	1*f*	1/3	2/3	1/2	0.0207(15)	1
Ge1	1*d*	2/3	1/3	1/2	0.0123(8)	1

four-fold unit cell, which we could compare to the 1 H structure would have the lattice parameters of a = 4.250(1) Å and c^* = 18.630/4 = 4.6575 Å which is slightly smaller than that of our structure, even though it has comparable Ga–Ge distance of 2.4696(6) Å. Evans *et al* [10] showed, from powder diffraction and Rietveld refinement, that SrGaGe crystallizes into the *P6/mmm* space group with unit cell parameters: a = 4.2718(1) Å and c = 4.7179(1) Å. The AlB_2-type structure has a single planar honeycomb layer with mixed Ga/Ge sites, sandwiched between the Sr atoms (1 H structure) with a distance between Ga and Ge atoms of 2.46632(6) Å. The authors suggest however, that a modulation of this structure might be present as electron diffraction experiment showed an additional reflections. The authors suggest a commensurate

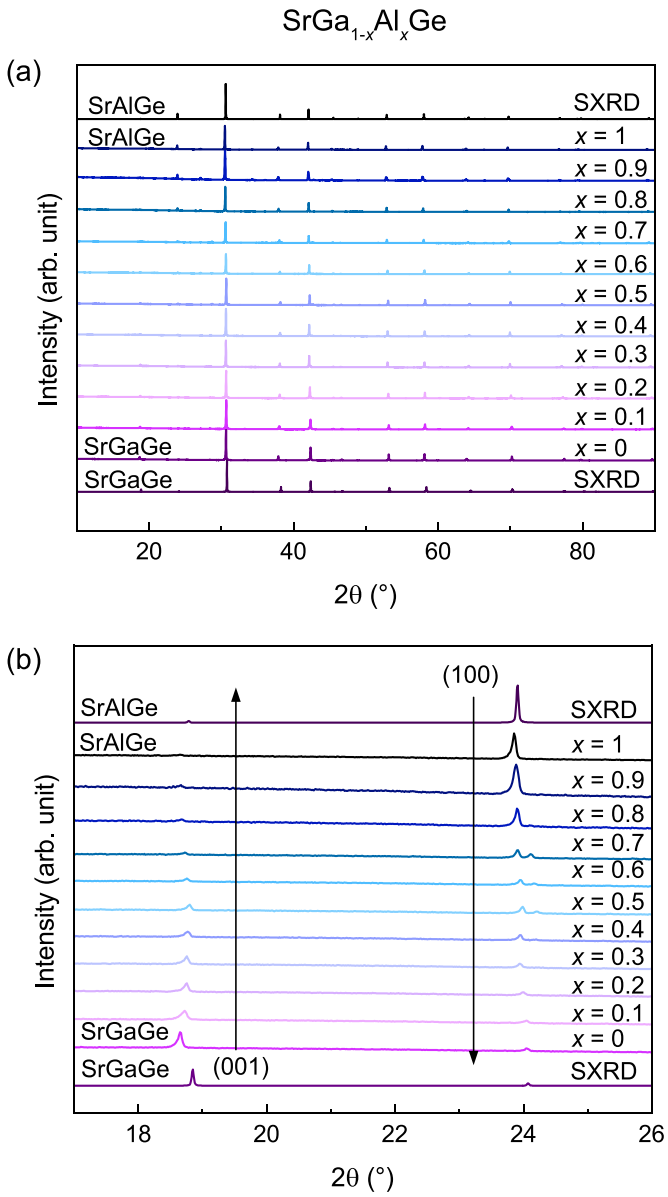

Figure 2. PXRD patterns for all members of the $SrGa_{1-x}Al_xGe$ ($0 < x < 1$) solid solution together with reference patters for SrGaGe (ICSD-166 385) and SrAlGe (ICSD-418 391). (a) PXRD patterns in the full 2θ range. (b) PXRD patterns in a 2θ range form 17° to 26° with focus on evolution of (001) and (100) Bragg peaks.

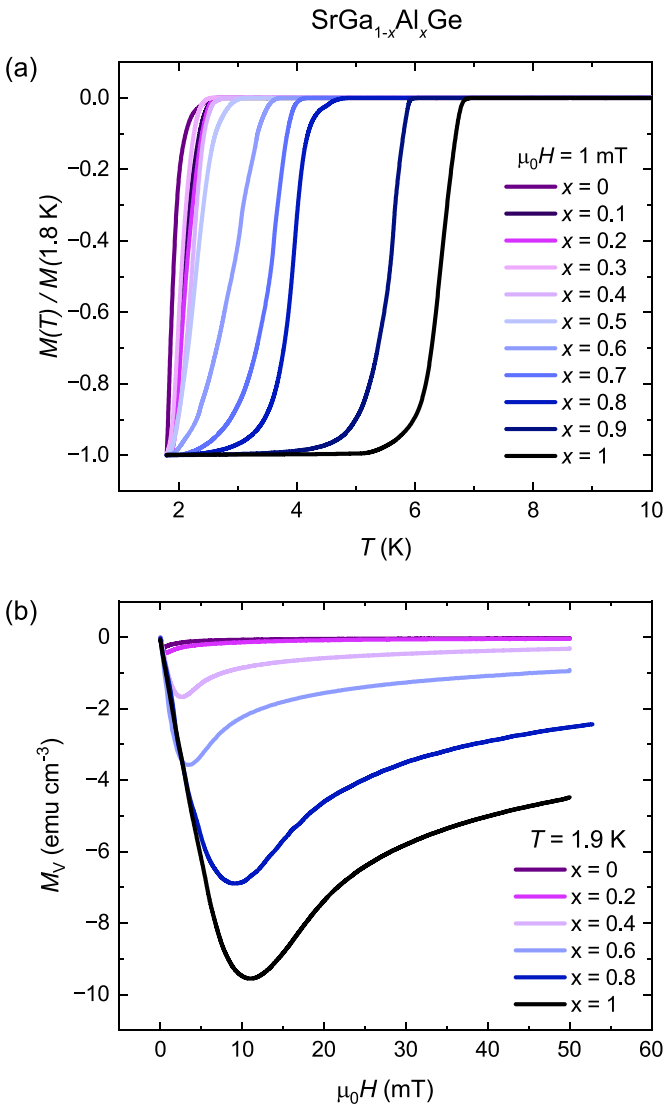

Figure 3. (a) Normalized ZFC temperature dependent magnetization *M(T)* data for all samples of the $SrGa_{1-x}Al_xGe$ solid solution. (b) Field dependent magnetization *M(H)* data for selected members of the solid solution measured at 1.9 K.

five-fold superstructure along the hexagonal *c* direction, however in their work, SrGaGe is still classified as the AlB_2-type structure.

The SXRD measurements for SrAlGe were refined in the $P\bar{6}m2$ space group (unit cell parameters: 4.2942(1) Å, c = 4.7200(2) Å, and the Al–Ge distance of 2.47926(6) Å), with the Al and Ge atoms clearly ordered in the planar honeycomb layers. The ordering of the Al and Ge atoms within the honeycomb layer is a reason for the non-centrosymmetry of the structure. The obtained result is in excellent agreement with earlier reports [10]. The crystal structures for SrGaGe and SrAlGe as obtained from SXRD are depicted in figure 1.

Details of the SXRD measurements and structural refinement are given in table 1, while the Wyckoff positions, the atomic coordinates, the equivalent isotropic displacement parameters, and the occupancy of the atoms in SrGaGe and SrAlGe are shown in table 2.

The PXRD patterns of the $SrGa_{1-x}Al_xGe$ samples ($0 \leqslant x \leqslant 1$) are shown in figure 2. All samples were found to be single phase. LeBail fits of the samples with $0 \leqslant x \leqslant 0.9$ were performed using the *P6/mmm* space group, while the last sample of the solid solution ($x = 1$) was refined with the $P\bar{6}m2$ space group, as only for this sample we have unambiguously confirmed an ordered structure by SXRD data.

Upon substitution of Ga by Al in $SrGa_{1-x}Al_xGe$, we observe a systematic exchange of the intensities between the (001) and (100) Bragg peaks. As shown in figure 2(b), the (001) Bragg peak is pronounced for SrGaGe and for the

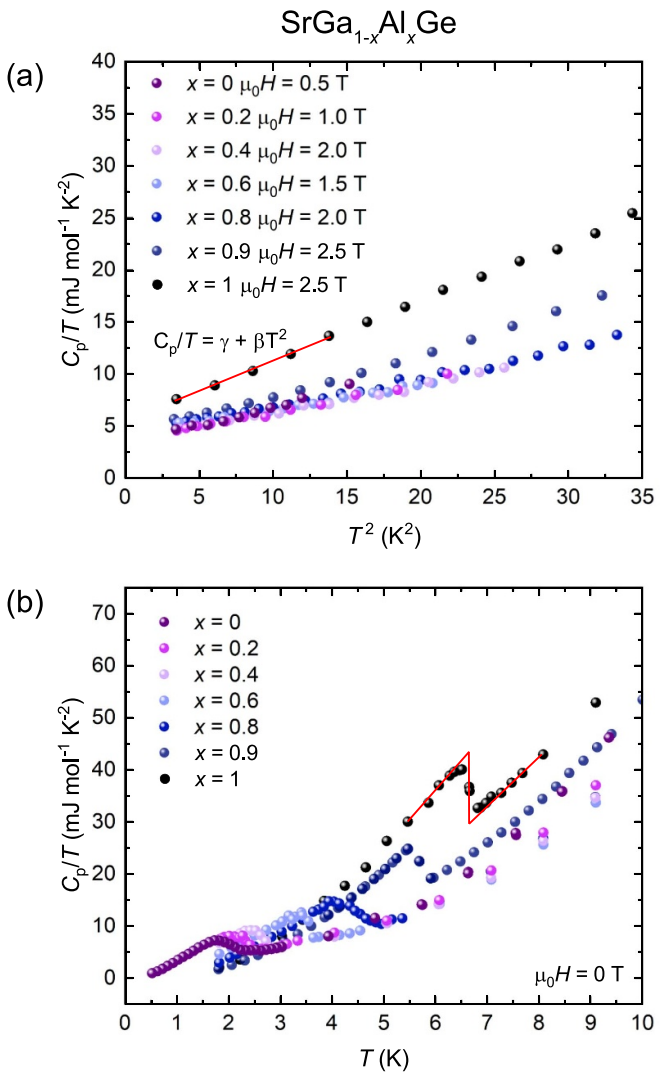

Figure 4. Heat capacity of selected samples of the $SrGa_{1-x}Al_xGe$ solid solution. (a) Normal state heat capacity measured in external magnetic field. (b) Heat capacity jump for selected samples and entropy conserving construction for a sample with $x = 1$.

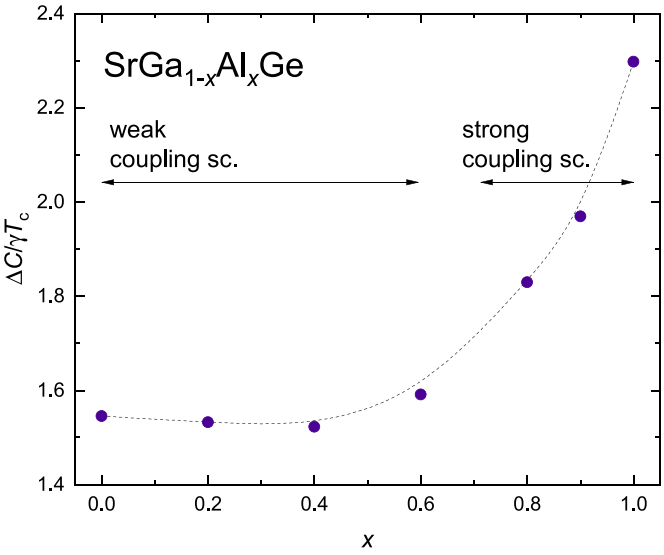

Figure 5. Values of the normalized heat capacity jump obtained from entropy conserving construction across the solid solution. The black dashed line is a guide to the eye.

samples with $x \leqslant 0.5$. For the samples with bigger content of Al ($0.5 < x \leqslant 1$) the Bragg peak (100) is systematically more pronounced, while the intensity of (001) peak decreases.

3.2. Physical properties

In figure 3(a), we show the zero field cooled (ZFC) temperature-dependent magnetization $M(T)$ in an external magnetic field of $\mu_0 H = 1$ mT measured for all members of the $SrGa_{1-x}Al_xGe$ solid solution. Data is presented as $M(T)/M(1.8\,\mathrm{K})$ for better comparability. The onset transition temperature T_c for SrGaGe and SrAlGe are found to be $T_c = 2.6$ K and 6.7 K respectively, in good agreement with previous reports [10]. As the composition shifts from SrGaGe to SrAlGe, the transition temperature rises continuously.

Figure 3(b) shows the volume magnetization isotherms $M_V(H)$ measured at 1.9 K for selected members of the solid solution with $x = 0$, 0.2, 0.4, 0.6, 0.8, and 1. The measurements confirm II-type superconductivity for the whole solid solution. We observed a systematic increase of the lower critical field H_{c1} with increasing x in agreement with the increase of the critical temperature T_c.

Specific heat capacity measurements of selected members of the $SrGa_{1-x}Al_xGe$ solid solution with $x = 0$, 0.2, 0.4, 0.6, 0.8, 0.9, and 1, were performed in order to provide thermodynamic evidence for the bulk nature of the superconductivity in these compounds. The heat capacity in the normal and superconducting state is shown in figure 4. At low temperatures, the total heat capacity can be considered as a sum of the electron and phonon contributions:

$$C_p = \gamma T + \beta T^3, \tag{1}$$

where γ is the Sommerfeld coefficient describing the electronic part and β describes the phonon part. The data in an applied external magnetic field together with the fit to equation (1) are shown in figure 4(a). Using the obtained β value, the Debye temperature Θ_D was calculated according to:

$$\Theta_D = \left(\frac{12\pi^4}{5\beta} nR\right)^{1/3}, \tag{2}$$

where n is the number of atoms per formula unit and $R = 8.31\,\mathrm{J\,mol^{-1}\,K^{-1}}$ is the ideal gas constant.

The Sommerfeld coefficient γ is shown in the table 3, and it increases as x increases. The Debye temperature Θ_D is shown in figure 7 as well as in the table 3 has a nonlinear behavior across the solid solution, which we discuss in details in the next section.

A pronounced discontinuity of the heat capacity at the temperatures in the vicinity of the transition to the superconducting state proves the bulk superconductivity for all measured samples (compare, e.g. references [26, 27]). By applying an

Table 3. Parameters obtained from heat capacity analysis for measured members of the $SrGa_{1-x}Al_xGe$ solid solution.

x	γ	β (mJ mol^{-2} K^{-4})	Θ_D	$\Delta C/\gamma T_c$	T_c	$\lambda_{e-p}^{(a)}$	$\lambda_{e-p}^{(b)}$
0	3.0(1)	0.37(1)	250(3)	1.55	2.05	0.53	0.68
0.2	3.64(6)	0.27(1)	278(4)	1.53	2.37	0.54	0.66
0.4	3.77(1)	0.25(1)	286(5)	1.52	2.67	0.55	0.65
0.6	4.18(1)	0.23(1)	292(6)	1.59	3.54	0.59	0.86
0.8	4.48(5)	0.232(6)	293(3)	1.83	4.47	0.62	0.94
0.9	4.59(6)	0.313(8)	265(2)	1.97	5.70	0.69	1.08
1	5.4(1)	0.583(9)	215(1)	2.30	6.65	0.80	1.40

Values of the λ_{e-p} calculated from (a) McMillan formula, (b) Allen–Dynes formula.

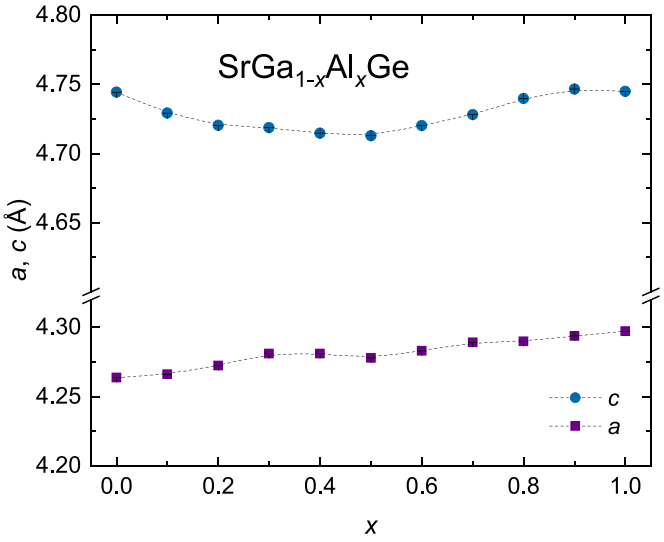

Figure 6. Unit cell parameters across the $SrGa_{1-x}Al_xGe$ solid solution. The black dashed lines are guides to the eye.

entropy conserving construction (see figure 7(b)) the exact value of the heat capacity jump defined as $\Delta C/\gamma T_c$ and the transition temperature T_c can be extracted. T_c obtained from the heat capacity measurements (table 3) increases across the solid solution and changes in the same fashion as the critical temperatures obtained from magnetization measurements. The normalized heat capacity jump increase across the solid solution are presented in figure 5(b) and in table 3. According to the BCS theory, the normalized heat capacity jump equals $\Delta C/\gamma T_c = 1.43$ for superconductors in the weak coupling limit. For SrGaGe the heat capacity jump equals 1.55 which is close to this theoretical value, indicating that SrGaGe is a superconductor falling into the weak coupling limit. The values of the heat capacity jump remains nearly constant for the Ga rich samples ($0 \leqslant x \leqslant 0.6$). For the samples with $x > 0.6$ the value of the normalized heat capacity jump increases up to $\Delta C/\gamma T_c = 2.30$, for SrAlGe. This value is far above previously reported theoretical value of 0.83 [28] as well as the theoretical BCS value, indicating that SrAlGe and the Al-rich samples of the solid solution are likely strong coupling superconductors.

The electron–phonon coupling constant λ_{e-p} was estimated by applying the semi-empirical McMillan formula, which is based on the phonon spectrum of niobium and is valid for $\lambda < 1.25$: [29]

$$\lambda_{e-p} = \frac{1.04 + \mu^* \ln(\Theta_D/1.45T_c)}{(1 - 0.62\mu^*)\ln(\Theta_D/1.45T_c) - 1.04}. \quad (3)$$

In this equation, Θ_D is the Debye temperature and μ^* is a parameter for the effective Coulomb repulsion that arises from Coulomb-coupling propagating much more rapidly than phonon coupling. The value of μ^* may vary from 1.0 to 1.8. Here, we use a value of $\mu^* = 0.13$, which is an average value used commonly for intermetallic superconductors (see, e.g., reference [30]). The calculated values of the electron–phonon coupling constant λ_{e-p}, using the McMillan formula are presented in figure 7 (purple squares) and discussed in detail in the next section. Additionally, values of the electron–phonon coupling constant λ_{e-p} calculated using McMillan formula for different values of μ^* are presented in the figure S2 in the SM.

For strong coupling superconductors, the electron–phonon coupling constant λ_{e-p} can be calculated using Allen–Dynes formula for T_c [31]:

$$T_c = \frac{\langle\omega_{log}^{\alpha^2 F}\rangle}{1.2}\exp\left[\frac{-1.04(1+\lambda_{e-p})}{\lambda_{e-p} - \mu^*(1+0.62\lambda_{e-p})}\right], \quad (4)$$

where $\langle\omega_{log}^{\alpha^2 F}\rangle$ is the logarithmic average phonon frequency estimated from the approximate formula for the specific heat jump in strongly coupled superconductors, and defined according to [32]:

$$\frac{\Delta C_p}{\gamma T_c} = 1.43\left[1 + 53\left(\frac{T_c}{\langle\omega_{log}^{\alpha^2 F}\rangle}\right)^2 \ln\left(\frac{\langle\omega_{log}^{\alpha^2 F}\rangle}{3T_c}\right)\right]. \quad (5)$$

The results of these calculations for λ_{e-p} for all members of the solid solution are presented in figure 7 (blue circles) and in the table 3.

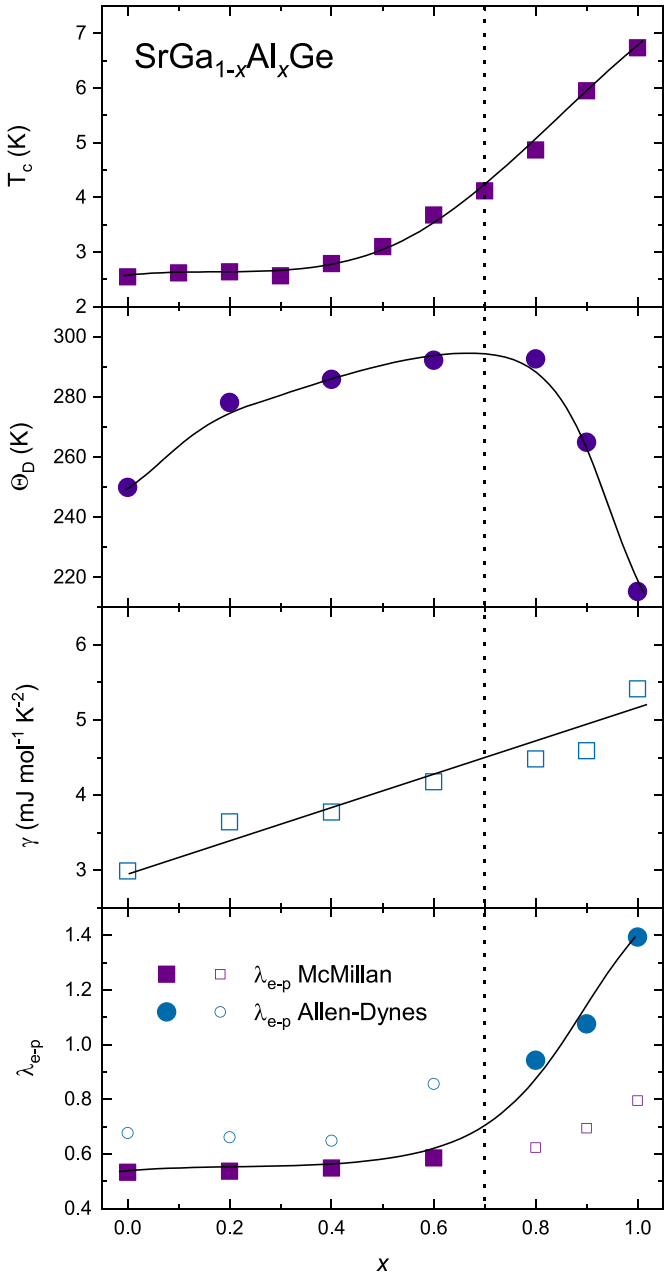

Figure 7. Superconducting parameters of the $SrGa_{1-x}Al_xGe$ solid solution. The upper panel presents the critical temperature T_c, obtained from the magnetic measurements. The middle panels present the Debye temperature Θ_D and Sommerfeld coefficient γ as obtained from the low-temperature fit in the normal state of the heat capacity. The last panel presents electron-phonon coupling constant λ_{e-p} calculated using the McMillan and the Allen–Dynes formula. Filled symbols indicate the values we consider accurate. The black lines are guides to the eye.

4. Discussion

The unit cell parameters extracted from the PXRD patterns are shown in figure 6. The unit cell parameters change slightly and non-linearly across the solid solution with a clear minimum in the c parameter for the sample with $x = 0.5$.

The superconducting transition temperature T_c, shown in the upper panel of figure 7 is found to change strongly in a non-linear fashion. The T_c changes very little in the first half of the solid solution e.i. from $x = 0$ to $x = 0.5$. For SrGaGe ($x = 0$) $T_c = 2.6$ K, while for $SrGa_{0.5}Al_{0.5}Ge$ ($x = 0.5$) the T_c was found to be 3.1 K. In the other half of the solid solution, we observe a rather steep increasing of the T_c. For $SrGa_{0.4}Al_{0.6}Ge$ ($x = 0.6$) $T_c = 3.7$ K, while for SrAlGe ($x = 1$) $T_c = 6.7$ K.

In order to understand better the superconductivity in this system, parameters which influence the T_c according to the BCS theory, i.e. Debye temperature Θ_D, Sommerfeld coefficient γ, and the electron–phonon coupling constant λ_{e-p} are plotted together in figure 7. Worth noticing is the behavior of the Debye temperature Θ_D which is changing in a non-linear fashion across the solid solution. The Debye temperature is equal to 250(3) K for SrGaGe and increases to 293(3) K for the sample with $x = 0.8$, then suddenly decreases for $x = 0.9$ and further reaches the value 215(1) K for SrAlGe. The Sommerfeld coefficient γ, presented in the middle panel of the figure 7, is correlated with the density of states at the Fermi levels and changes linearly across the solid solution. Last, but not least, the calculated values of the electron–phonon coupling constant λ_{e-p} using the inverted McMillan formula as well as the Allen–Dynes formula are presented in the bottom panel of figure 7. The McMillan formula is commonly considered to be more accurate for weakly coupled superconductors, while the Allen–Dynes formula allows for the estimation of electron–phonon coupling strength of strongly coupled superconductors [33]. The filled symbols in figure 7 indicate the values we consider accurate, i.e. below $x \leqslant 0.6$ the McMillan formula and $x > 0.6$ the Allen–Dynes formula.

Our results suggest that small increase of the T_c at the beginning of the solid solution (i.e. samples with x from 0 to 0.5) might be associated with the increase of the Debye temperature Θ_D, as well as the increase of the density of states at the Fermi level, what can be observed by the increase of the Sommerfeld coefficient γ. The other half of the solid solution seems to show a more complex interplay between these parameters. For samples with $x > 0.5$ we observe a significant increase of T_c. While the γ is still linearly increasing, the Θ_D starts to decrease, what should cause decrease of the T_c. However, for these samples the values of the electron–phonon coupling constant λ_{e-p} start to significantly increase and seems to have the strongest influence on T_c in the system.

5. Conclusion

In this work, a detailed analysis of the structure and the superconducting properties of SrGaGe, SrAlGe, and the $SrGa_{1-x}Al_xGe$ solid solution was presented. We showed a refined structural model for SrGaGe, which crystallizes in the *P6/mmm* space group with the unit cell parameters $a = 4.2555(2)$ Å, and $c = 4.7288(2)$ Å, and local-disorder around the mirror plane along the c-axis, which can be interpreted as a slight buckling of the honeycomb layer. We confirmed that SrAlGe crystallizes in the non-centrosymmetric $P\bar{6}m2$ space group with unit cell parameters $a = 4.2942(1)$ Å, and $c = 4.7200(2)$ Å, with an ordered honeycomb lattice. Both compounds are superconductors with critical temperatures

of $T_c = 2.6$ and 6.7 K, respectively, as shown by magnetization measurements. Using specific heat measurements, we have proven the bulk nature of superconductivity and revealed that SrGaGe is a superconductor in the weak coupling limit, while SrAlGe is a strong coupling non-centrosymmetric superconductor.

By preparing the $SrGa_{1-x}Al_xGe$ solid solution, we investigated the continuous transition between those two crystal structures and different electronic states. We showed that the unit cell parameters and transition temperatures change in a non-monotonic way. The biggest increase in the transition temperature happens in the Al rich compositions of the solid solution. Parameters derived from heat capacity measurements also change in a non-linear way, and the most striking is a change of the Debye temperature, which is increasing for the samples from $x = 0$ to 0.8 and then suddenly decreases for the last two members of the solid solution. However, our results suggest that the strongest contribution to the transition temperature T_c in this system has the electron–phonon coupling constant λ_{e-p}, which was analyzed across the solid solution using the McMillan formula for the samples with $0 \leqslant x \leqslant 0.6$, while for the three last members of the solid solution we used the Allen–Dynes formula, for strong coupling superconductors. This decision was dictated by the high values of λ_{e-p} obtained from the McMillan formula, as well as the high value of the heat capacity jump, which is by far crossing the limit of the 1.43 value of the BCS theory.

Hence, across the solid solution we observed a transition from the weak- to strong-coupling superconductivity, which may be associated with the rearrangement of the atoms within the honeycomb lattice as indicated by the distinctively different values of the Debye temperature. We have revealed a disorder-to-order transition connected with the loss of an inversion center in the honeycomb layer, which increased the electron–phonon coupling and enhanced the superconductivity across the solid solution.

Data availability statement

All data for this study is available in the article and the SM. The crystal structures are made available via the CCDC. Further data of this study are made available upon reasonable request from the authors.

Acknowledgment

This work was supported by the Swiss National Science Foundation under Grant No. PCEFP2_194183.

ORCID iDs

Dorota I Walicka https://orcid.org/0000-0001-8482-766X
Olivier Blacque https://orcid.org/0000-0001-9857-4042
Tomasz Klimczuk https://orcid.org/0000-0002-7089-4631
Fabian O von Rohr https://orcid.org/0000-0003-0422-6042

References

[1] Cao Y, Fatemi V, Fang S, Watanabe K, Taniguchi T, Kaxiras E and Jarillo-Herrero P 2018 Unconventional superconductivity in magic-angle graphene superlattices *Nature* **556** 43
[2] Nagamatsu J, Nakagawa N, Muranaka T, Zenitani Y and Akimitsu J 2001 Superconductivity at 39 K in magnesium diboride *Nature* **410** 63
[3] Sigrist M and Ueda K 1991 Phenomenological theory of unconventional superconductivity *Rev. Mod. Phys.* **63** 239
[4] Smidman M, Salamon M B, Yuan H Q and Agterberg D F 2017 Superconductivity and spin–orbit coupling in non-centrosymmetric materials: a review *Rep. Prog. Phys.* **80** 036501
[5] Bauer E and Sigrist M 2012 *Non-Centrosymmetric Superconductors: Introduction and Overview* vol 847 (Springer)
[6] von Rohr F O 2023 Chemical principles of intrinsic topological superconductors *Chem. Mater.* **35** 9455
[7] Nishikubo Y, Kudo K and Nohara M 2011 Superconductivity in the honeycomb-lattice pnictide SrPtAs *J. Phys. Soc. Japan* **80** 055002
[8] Biswas P K *et al* 2013 Evidence for superconductivity with broken time-reversal symmetry in locally noncentrosymmetric SrPtAs *Phys. Rev.* B **87** 180503
[9] Fischer M H, Neupert T, Platt C, Schnyder A P, Hanke W, Goryo J, Thomale R and Sigrist M 2014 Chiral d-wave superconductivity in SrPtAs *Phys. Rev.* B **89** 020509
[10] Evans M J, Wu Y, Kranak V F, Newman N, Reller A, Garcia-Garcia F J and Häussermann U 2009 Structural properties and superconductivity in the ternary intermetallic compounds MAB (M = Ca, Sr, Ba; A = Al, Ga, In; B = Si, Ge, Sn) *Phys. Rev.* B **80** 064514
[11] Shein I R, Medvedeva N I and Ivanovskii A L 2003 Band structure of new superconducting AlB_2-like ternary silicides $M(Al_{0.5}Si_{0.5})_2$ and $M(Ga_{0.5}Si_{0.5})_2$ (where M = Ca, Sr and Ba) *J. Phys.: Condens. Matter* **15** L541
[12] Mazin I I and Papaconstantopoulos D A 2004 Electronic structure and superconductivity of CaAlSi and SrAlSi *Phys. Rev.* B **69** 180512
[13] Imai M, Nishida K, Kimura T and Abe H 2002 Superconductivity of $Ca(Al_{0.5}Si_{0.5})_2$, a ternary silicide with the AlB_2-type structure *Appl. Phys. Lett.* **80** 1019
[14] Walicka D I, Lefèvre R, Blacque O, López-Paz S A, Rischau C W, Cervellino A, Triana C A and von Rohr F O 2023 Structural phase transition and superconductivity in 2H-BaGaGe with buckled honeycomb layers *Phys. Rev. Mater.* **7** 074805
[15] Lorenz B, Lenzi J, Cmaidalka J, Meng R L, Sun Y Y, Xue Y Y and Chu C W 2002 Superconductivity in the C32 intermetallic compounds $AAl_{2-x}Si_x$, with A = Ca and Sr; and $0.6 < x < 1.2$ *Physica* C **383** 191
[16] Lorenz B, Cmaidalka J, Meng R L and Chu C W 2003 Thermodynamic properties and pressure effect on the superconductivity in CaAlSi and SrAlSi *Phys. Rev.* B **68** 014512
[17] Walicka D I, Guguchia Z, Lago J, Blacque O, Ma K, Liu H, Khasanov R and von Rohr F O 2021 Two-gap to single-gap superconducting transition on a honeycomb lattice in $Ca_{1-x}Sr_xAlSi$ *Phys. Rev. Res.* **3** 033192
[18] Czybulka A, Pinger B and Schuster H-U 1989 Neue Erdalkali-Gallium-Silicide, -Germanide und -Stannide mit vom AlB_2-Typ abgeleiteten Strukturen *Z. Anorg. Allg. Chem.* **579** 151
[19] Youn S and Freeman A 2012 Electronic structure and properties of BaAlGe and SrAlGe *Physica* C **476** 54

[20] Rodríguez-Carvajal J 1993 Recent advances in magnetic structure determination by neutron powder diffraction *Physica* B **192** 55
[21] Clark R C and Reid J S 1995 The analytical calculation of absorption in multifaceted crystals *Acta Crystallogr.* A **51** 887
[22] Dolomanov O V, Bourhis L J, Gildea R J, Howard J A K and Puschmann H 2009 OLEX2: A complete structure solution, refinement and analysis program *J. Appl. Crystallogr.* **42** 339
[23] Sheldrick G M 2015 SHELXT-Integrated space-group and crystal-structure determination *Acta Crystallogr.* A **71** 3
[24] Sheldrick G M 2015 Crystal structure refinement with SHELXL *Acta Crystallogr.* C **71** 3
[25] Spek A L 2009 Structure validation in chemical crystallography *Acta Crystallogr. sec.* D **65** 148
[26] von Rohr F, Nesper R and Schilling A 2014 Superconductivity in rubidium-substituted $Ba_{1-x}Rb_xTi_2Sb_2O$ *Phys. Rev.* B **89** 094505
[27] von Rohr F, Winiarski M J, Tao J, Klimczuk T and Cava R J 2016 Effect of electron count and chemical complexity in the Ta-Nb-Hf-Zr-Ti high-entropy alloy superconductor *Proc. Natl Acad. Sci.* **113** E7144
[28] Djelloul M, Bouderba H, Beddiaf R, Bentria B and Helifa B 2021 About the ground state structure and superconductivity of the SrAlGe compound *Physica* C **584** 1353868
[29] McMillan W L 1968 Transition temperature of strong-coupled superconductors *Phys. Rev.* **167** 331
[30] Ma K, Gornicka K, Lefèvre R, Yang Y, Rønnow H M, Jeschke H O, Klimczuk T and von Rohr F O 2021 Superconductivity with high upper critical field in the cubic centrosymmetric η-carbide $Nb_4Rh_2C_{1-\delta}$ *ACS Mater. Au* **1** 55
[31] Allen P B and Dynes R C 1975 Transition temperature of strong-coupled superconductors reanalyzed *Phys. Rev.* B **12** 905
[32] Marsiglio F and Carbotte J P 1986 Strong-coupling corrections to Bardeen-Cooper-Schrieffer ratios *Phys. Rev.* B **33** 6141
[33] Webb G, Marsiglio F and Hirsch J 2015 Superconductivity in the elements, alloys and simple compounds *Physica* C **514** 17